Double power-law universal scaling function for the distribution of waiting times in labquake catalogues

Honglian Li and Emma Valdés
Departament de Física de la Matèria Condensada,
Facultat de Física, Universitat de Barcelona,
Martí i Franquès 1, 08028 Barcelona, Catalonia

Eduard Vives*
Departament de Física de la Matèria Condensada,
Facultat de Física, Universitat de Barcelona,
Martí i Franquès 1, 08028 Barcelona, Catalonia, (Spain)
(Dated: September 10, 2024)

We postulate that waiting times between avalanches in self-organized critical systems are distributed according to a universal double power-law probability density. This density is defined by two critical exponents α and β characterizing the distribution of short ($\sim \delta^{-\alpha}$) and long ($\sim \delta^{-\beta}$) waiting times, and a crossover parameter δ_0 which separates the two behaviours in a sharp shoulder. This crossover parameter depends on the system properties as well as on the observation conditions. It can be used as a scaling factor that transforms the distributions into a universal scaling law as proposed by Per Bak. We use experimental data from labquake catalogues (Acoustic Emission events) obtained during the uniaxial compression of a number of charcoal samples with different hardnesses, and different energy thresholds. To obtain good fits it is essential that the catalogues are long enough to include a representative critical mixture of periods with different avalanche rates. In all the cases studied, individual maximum likelihood analysis allows the exponents α and β and the crossover parameter δ_0 to be fitted. This parameter shows a clear dependence with the energy threshold that can be explained from the Gutenberg-Richter law for the avalanche energy distributions. The observed variations of the exponents α and β fall within the sample-to-sample variability which suggest that these values could be universal. We estimate mean values $\alpha = 0.9 \pm 0.1$ and $\beta = 2.0 \pm 0.3$ from the full set of recorded experimental data. These values are close to the combination $\alpha = 1$, $\beta = 2$, which exhibits a special mathematical cancellation of singularities.

I. INTRODUCTION

Complex systems with spatial and temporal degrees of freedom that are smoothly driven by an external field often respond intermittently by a sequence of stochastic burst events called avalanches [1]. Those are fast relaxations separated by long silent waiting times.

The classical Self Organized Criticality (SOC) paradigm introduced by Per Bak [2] as well as other holistic approaches [3] suggest that some complex systems reach a dynamic non-equilibrium critical state with lack of characteristic scales. Most of the details of the microscopic physical interactions in the system become irrelevant, and the laws governing avalanche response are expected to depend on very few dimensionless parameters (typically exponents) showing a certain degree of universality.

These approaches usually start by reducing the complexity of the sequence of burst events to a temporal point process with avalanches occurring at times t_k and exhibiting different avalanche properties: location, energy E_k, size, duration, etc.

Avalanche properties and occurrence times are considered to be stochastic and, consequently, they are described by probability densities that might reflect the existence or not of correlations between them.

The experimental data (or historical observations) are recorded in catalogues (for instance a list of energy events $\{t_k, E_k\}$) that can be used to compare with the proposed mathematical laws or to fit some of their theoretical parameters. The catalogues are usually constrained to a certain spatial region $\mathcal{R}$, to a certain temporal window $\mathcal{T}$ and to an energy observation window $\mathcal{E}$ (typically only energies above a threshold E_{th} are recorded).

The most famous holistic laws in geophysics is Gutenberg-Richter (GR) law [4] that reveals that earthquake energies (seismic moments) are power-law distributed ($dP(E) \propto E^{-\epsilon} dE$) with a rather universal exponent $\epsilon \simeq \frac{5}{3} \simeq 1.67$.

Similarly, Omori law [5] reflects the existence of time correlations between consecutive earthquakes: after a big event in a certain location there is an increase of the activity rate in the nearby region above the background rate. These extra events are called aftershocks and are reflected in the fact that (in a given region and

* eduard@fmc.ub.edu; Also at University of Barcelona Institute of Complex Systems (UBICS), Barcelona, Catalonia

for a given period of time) waiting times become statistically shorter than those corresponding to independent Poissonian events.

A much more recent law reflecting the existence of time correlations in the earthquake sequences is the Universal Scaling Law (USL), introduced by P. Bak et al. [6] and, shortly afterwards, revised by A. Corral [7]. This law refers to the distribution of waiting times ($\delta_k = t_{k+1} - t_k, k = 1, \cdots, N$). The probability density for observing δ values within a certain interval will be described by $dP(\delta) = D_{\mathcal{R},\mathcal{T},\mathcal{E}}(\delta)d\delta$.

Not only the physical properties of the systems, but also the observational limitations of the catalogues influence the recorded waiting times. We clearly expect that enlarging the observed spatial region $\mathcal{R}$ will imply to have more events being recorded in the catalogue and thus in general shorter waiting times. Similarly, increasing the threshold E_{th} will reduce the number of events and thus increase the waiting times.

The USL hypothesis proposed that all the dependencies with the time-space-energy observational window ($\mathcal{T} - \mathcal{R} - \mathcal{E}$) can be accounted for by a single scalar parameter, either a characteristic rate r_c or a characteristic time δ_c, so that the following scaling relation is fulfilled

$$D_{\mathcal{R},\mathcal{T},\mathcal{E}}(\delta)d\delta = \Phi(\delta/\delta_c)d\delta/\delta_c = \Phi(r_c\delta)r_c d\delta \quad (1)$$

where $z = \delta/\delta_c$ (or $z = r_c\delta$) is the scaled waiting time, and $\Phi(z)$ is the scaling function that does not depend on the observational window ($\mathcal{T}-\mathcal{R}-\mathcal{E}$).

The validity of the USL as well as the precise shape of $\Phi(z)$ has been extensively discussed [7–17]. Despite the existence of some exact theorems that apparently demonstrated that the USL hypothesis could not be correct [9, 13], the reality is that at present it has been incorporated in many models even for earthquake risk assessment [18, 19].

It is evident that for a hypothetical Poisson process with totally uncorrelated events we should have $\Phi(z) = e^{-z}$. A log-log plot of the histogram of the scaled experimental waiting times ($z_k = \delta_k/\delta_0$) will show a flat behaviour for $z \ll 1$ and a fast exponential decay for $z \gg 1$.

But in reality events are Omori-correlated and, as explained above, there is an increase in the frequency of small values of δ relative to the flat Poisson behaviour. The observed histograms in the $z \ll 1$ region are therefore better described by the scaling function $\Phi(z) = z^{-\alpha}e^{-z}$. Regarding the decay in the $z \gg 1$ region, many recorded catalogues indeed show histograms with an exponential decay. However, it was suggested that when catalogues reflect rich enough mixtures of temporal windows with high and low activity [20], the $z \gg 1$ tail may transform in a second power-law $\Phi(z) \sim z^{-\beta}$. The main problems for observing such a mixture of rates can be (i) that most available catalogues tend to concentrate in spatial regions where earthquakes occur thus neglecting the contribution of low rate regions and (ii) that the recorded time periods are restricted to less than a century (or even less than 25 years is we only consider complete catalogues without under-counting of small events).

Twelve years ago [20] it was proposed that Acoustic Emission (AE) events (also called hits, after detection) obtained during the uniaxial compression of porous materials had strong statistical similarities with earthquake data. The so-called labquakes show a power-law (GR like) distribution of energies, Omori correlations and waiting times that fulfill the USL. These experiments have several advantages when compared to earthquakes: (i) there is major control of experimental parameters and (ii) they allow for a systematic repetition with samples with *a priori* identical properties. This may help in the understanding of the statistical sample-to-sample fluctuations that cannot be studied from observations of real earthquakes.

Among the different studied porous samples, a recent work [21] focused on charcoal. These samples allow for the study of large labquake catalogues usually exhibiting time periods of fluctuating rates and with a very well defined GR exponent $\epsilon = 1.64$, in very good numerical agreement with the values found in real earthquake catalogues.

In the present work we will present a study of the compression of 17 commercial charcoal samples of similar sizes and four different nominal hardnesses. From each experiment, AE hit catalogues will be built using seven different energy thresholds. This gives a total of ~ 100 catalogues for a systematic statistical analysis.

We will fit the data sets with a pure double power-law distribution with three parameters: two exponents and the crossover parameter δ_0. This parameter will be used to scale the waiting times and to reveal that distributions follow the universal scaling law. The hypothesis that we are testing is not only that the behaviours of $\Phi(z)$ are power-law in the $z \ll 1$ and $z \gg 1$ region but that the full shape can be described by a pure double power-law with a sharp crossover at $z = 1$ ($\delta = \delta_0$).

The paper is organized as follows. In the next section II we discuss about theoretical probability densities that can be used to model "critical" avalanche properties with scale invariance. We compare the mathematical properties of the standard power-law density with the proposed double power-law density. In section III we discuss the details of the AE detection of labquakes. In section IV we show the fit of the double-power-law model to the data using the maximum likelihood method and its scaling properties. Finally in section V we summarize and conclude.

II. SCALE INVARIANT PROBABILITY DENSITIES: POWER-LAWS AND DOUBLE POWER-LAWS

In equilibrium critical phenomena, universal laws governing the system response are described by power-law functions $f(x) = Ax^{\alpha}$ (where A is an amplitude, α is a critical exponent and x is a measure of the relative distance to the critical point, along the temperature axis $(T-T_c)/T_c$ or along the external field $(H-H_c)/H_c$). This function $f(x)$ fulfills the mathematical condition of scale invariance:

$$f(\lambda x) = \lambda^{\alpha} f(x) \ \ \forall \lambda \in \Re^{+} \tag{2}$$

where λ is a dilatation factor.

By analogy, when modelling the stochastic avalanche properties close to a non-equilibrium critical point, power-law probability densities are chosen [22]. These are also called Pareto probability densities [23]. For a generic positive and continuum property $x > 0$ (such as the avalanche size, the avalanche energy, etc.) the probability of measuring a value in the infinitesimal interval $(x, x+dx)$ is given by $dP = g(x)dx$ with

$$g(x;\epsilon,x_0) = \begin{cases} 0 & \text{if } x < x_0 \\ \dfrac{\epsilon-1}{x_0}\left(\dfrac{x}{x_0}\right)^{-\epsilon} & \text{if } x \geq x_0 \end{cases} \tag{3}$$

where we indicate the density parameters after the the semicolon: ϵ is the critical exponent and x_0 is a minimum cutoff. Note that the normalization condition requires on the one hand the existence of the cutoff $x_0 > 0$ and, on the other hand, that the exponent fulfills $\epsilon > 1$.

In general not much attention is paid to the meaning of x_0. Often it is justified as having an experimental origin (minimum detection threshold of the property x) or it can simply be understood as an indication that an avalanche cannot have its physical properties (size, amplitude, energy) being null.

Note that if the expected value $\langle x \rangle$ exists (only when $\epsilon > 2$) then it turns to be proportional to the cutoff x_0:

$$\langle x \rangle = \frac{\epsilon-1}{\epsilon-2} x_0 \tag{4}$$

Thus the expected value of avalanche properties in critical systems depends on the minimum detection threshold for the observation. The smaller the avalanches one is able to observe, the smaller the expected value will be.

A particular unsatisfactory aspect concerning this theoretical probability density should be noted: the existence of a cutoff breaks the mathematical global scale invariant condition (2). For any value of x it is possible to find a scaling factor λ that moves $x \to \lambda x$ below x_0 and thus violates condition (2).

The problem is worse if the power-law probability density is used to model, not the avalanche properties, but the waiting times between avalanches δ. In this case, it would be desirable that the proposed probability density could be normalized in the interval $[0,\infty)$ since, *a priori* , there is no physical reason why two avalanches cannot occur exactly at the same time in different places of the system. One is then forced to consider other theoretical probability densities having a minimum number of non-universal parameters and being as "scale invariant" as possible.

A very simple candidate is the double power-law probability density. It was introduced much more recently than the Pareto probability density for the study of the income distribution [24] in economics. Since then it has been used to describe different phenomena in complex systems [25, 26].

It can be written as:

$$g(\delta;\alpha,\beta,\delta_0) = \begin{cases} \dfrac{(1-\alpha)(\beta-1)}{(\beta-\alpha)\delta_0}\left(\dfrac{\delta}{\delta_0}\right)^{-\alpha} & \text{if } 0 < \delta \leq \delta_0 \\ \dfrac{(1-\alpha)(\beta-1)}{(\beta-\alpha)\delta_0}\left(\dfrac{\delta}{\delta_0}\right)^{-\beta} & \text{if } \delta_0 < \delta < \infty \end{cases} \tag{5}$$

In this case the density has three parameters: two power-law exponents, α for the small values of the variable and β for the large values, and the crosover parameter δ_0. The condition for the probability density to be normalized in the whole range $0 \le \delta < \infty$ is that $\alpha < 1$ and $\beta > 1$.

It could be argued that the parameter δ_0 in this case is a characteristic scale of the problem and thus this is not a probability density describing a situation without lack of characteristic scales. But note that the role of δ_0 is not very different from the role of x_0 in the standard power-law probability density. As we will see, it is essentially controlled by the experimental limitations of each catalogue (detection threshold, maximum observation time, etc.). In the case that the expected value $\langle\delta\rangle$ exists, (when $\beta > 2$) one finds also a similar situation (but not worse) than with the standard power-law:

$$\langle\delta\rangle = \frac{(1-\alpha)(\beta-1)}{(2-\alpha)(\beta-2)}\delta_0 \tag{6}$$

It is also interesting to note that the double power-law probability density includes, as a particular case, the standard power-law: it corresponds to the case $\alpha \to -\infty$. The δ_0 parameter, then, becomes the minimum cutoff.

A property that makes this proposed probability density very interesting is the fact that one can consider the inverse of the waiting times $r = 1/\delta$ as the instantaneous estimates of the avalanche rates. One cannot measure the instantaneous rate in a time interval shorter than the interval between two consecutive avalanches in the catalogue. It seems plausible that a "critical" system should have neither any characteristic waiting time nor any characteristic rate. Thus both distributions for δ and for r should somehow show good "critical" properties.

If one transforms the double power-law probability density by changing the variables to $\delta \to r = 1/\delta$, one nicely gets a new double power-law

$$g(r;\gamma,\eta,r_0) = \begin{cases} \dfrac{(1-\gamma)(\eta-1)}{(\eta-\gamma)r_0}\left(\dfrac{r}{r_0}\right)^{-\gamma} & \text{if } 0 < r \le r_0 \\[2ex] \dfrac{(1-\gamma)(\eta-1)}{(\eta-\gamma)r_0}\left(\dfrac{r}{r_0}\right)^{-\eta} & \text{if } r_0 < r < \infty \end{cases} \tag{7}$$

with an exponent $\gamma = 2-\beta$ for small rate values, $\eta = 2-\alpha$ for large rate values and $r_0 = \frac{1}{\delta_0}$. The conditions for the normalization of $g(\delta)$ ($\alpha < 1$ and $\beta > 1$) imply that $g(r)$ is also well normalized ($\gamma = 2-\beta < 1$ and $\eta = 2-\alpha > 1$).

Note however that the conditions for the existence of the expected values $\langle\delta\rangle$ and $\langle r\rangle$ are different. Depending on the values of α and β (and the corresponding γ and η) we find the four cases indicated in the exponent diagram in Fig. 1

Before concluding this theoretical section it should be mentioned that the combination of exponents $\alpha = 1$ and $\beta = 2$ (which will be relevant in the experimental analysis) fullfills a special mathematical cancellation of singularities that might have some physical relevance.

When $\alpha = 1$ the double power-law probability density is marginally not well defined since the normalization diverges. When $\beta = 2$ the average $\langle\delta\rangle$ is, also, marginally not well defined. Nevertheless, even for a not well normalized distribution, one could write the average waiting time as

$$\langle\delta\rangle = \frac{\int_0^\infty \delta\, g(\delta)d\delta}{\int_0^\infty g(\delta)d\delta} = \frac{\int_0^{\delta_0} \delta\, g(\delta)d\delta + \int_{\delta_0}^\infty \delta\, g(\delta)d\delta}{\int_0^{\delta_0} g(\delta)d\delta + \int_{\delta_0}^\infty g(\delta)d\delta} = \delta_0 \frac{\int_0^1 z^{1-\alpha}dz + \int_1^\infty z^{1-\beta}dz}{\int_0^1 z^{-\alpha}dz + \int_1^\infty z^{-\beta}dz} \tag{8}$$

where, in the last equality, we have performed the change of variables $z = \delta/\delta_0$ ($dz = d\delta/\delta_0$). Now, in the second integral in the numerator and the denominator, one can perform the change of variables $x = 1/z$ ($dx = -1/z^2 dz$):

$$\langle\delta\rangle = \delta_0 \frac{\int_0^1 z^{1-\alpha}dz + \int_0^1 x^{-1+\beta-2}dx}{\int_0^1 z^{-\alpha}dz + \int_0^1 x^{\beta-2}dx} = \delta_0 \frac{\int_0^1 dz + \int_0^1 x^{-1}dx}{\int_0^1 z^{-1}dz + \int_0^1 dx} = \delta_0 \tag{9}$$

where, in the last step, we have set $\alpha = 1$ and $\beta = 2$. The divergences in the numerator and

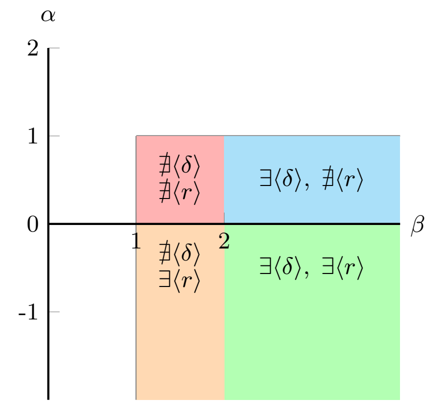

Figure 1. The coloured area shows the regions of the α-β diagram where the double power-law probability density is well defined. Moreover, the four different colours show the regions where the expected waiting time values $\langle\delta\rangle$ and the expected instantaneous rate values $\langle r\rangle$ exist or not, as indicated by the labels. The blue, orange and green regions extend towards the right and towards the bottom.

denominator cancel out and we obtain a finite $\langle\delta\rangle = \delta_0$ resolving the ∞/∞ singularity in Eq.6.

III. EXPERIMENTAL

The studied samples have been obtained from commercial charcoal sticks (Nitram Art Inc.) corresponding to four different nominal hardnesses: H, HB, B and B^+. The sticks are elongated parallelepipeds with approximately square crossections between 27 and 44 mm^2 .

Each sample has been cut from the stick using a blade with an approximate height of 9-12 mm and slightly polished with sand paper to obtain parallel upper and lower faces. Tab. I shows the properties of the 17 studied samples. Note that the density (which varies by more than a 100%) is clearly correlated with the nominal hardness.

The specimens have been compressed between two aluminium plates, driven at a constant speed of 0.02 mm/min by a Zwick/Roell testing machine with electronic speed control. The compression plates contain embedded piezoelectric transducers with 9.5 mm diameter, centered on the sample, at 2 mm distance from it. The good ultrasonic contact between the transducers and the plates, as well as between the plates and the sample is ensured by a thin film of Vaseline.

The voltage signals detected by the transducers are first pre-amplified (60 dB) and sent to two separate channels of a PCI2 system from Europhysical Acoustics. Individual AE events are defined/separated by using a threshold of 23 dB. The threshold is selected as low as possible, while ensuring that noise signals are not detected when the sample is not being compressed.

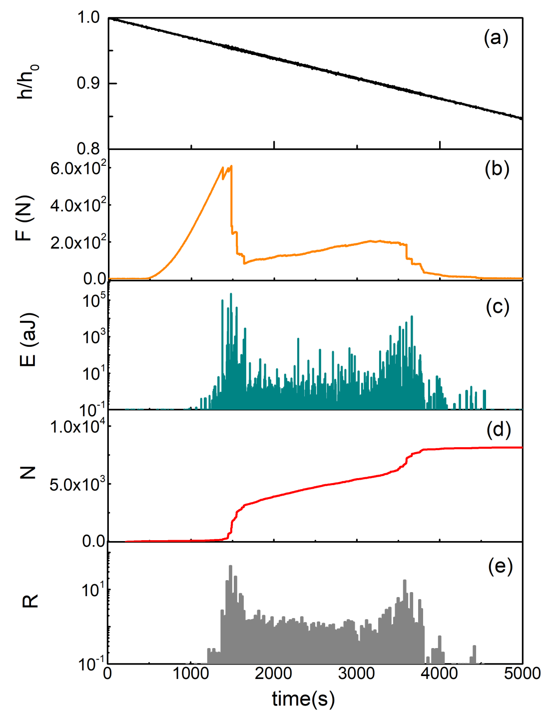

Figure 2. Example of the recorded data from sample HB_1 as a function of time. (a) Compressive strain; (b) force; (c) hit energies; (d) cumulative number of recorded hits; (e) rate evolution evaluated as the number of hits every 20 s.

AE hits are defined by the standard procedure: hits start when the voltage signal crosses the threshold, and finish when the voltage remains below threshold for more than 200 μs. The energy of the hit is measured as the time integral of the squared voltage during the whole event, divided by a reference resistance of 10 kΩ. More details of the experimental setup can be found in [21].

In each experiment we have selected the hits only from the channel that recorded a larger number of them, thus revealing a better acoustic contact with the sample, and avoiding double counting of large hits that are simultaneously recorded by both transducers. The number of hits recorded in each experiment are detailed in Tab. I. Note that, in general, the number of hits increases when the hardness decreases, but there is a high variability. This is due to the fact that the coupling of the transducers to the sample (as well as other attenuation factors) can be very different from one experiment to another.

Fig. 2 shows a summary of the results corresponding to a typical experiment (HB_1).

sample name	nominal hardness	crossection (mm^2)	height (mm)	m (mg)	density (g/cm^3)	AE hits	N $E_{th} = 0.5$ aJ
H_1	H	34.12	11.49	0.243	619.83	3663	1027
H_2	H	34.39	11.35	0.235	602.07	15076	4786
H_3	H	33.95	11.45	0.242	622.47	1347	416
H_4	H	33.87	10.52	0.214	601.89	860	250
HB_1	HB	43.7	10.88	0.197	414.37	8261	1902
HB_2	HB	43.82	10.69	0.2	426.96	24687	6630
HB_3	HB	43.26	9.88	0.173	404.77	34213	8670
HB_4	HB	43.01	10.43	0.184	410.22	21010	5337
B_1	B	39.98	11.51	0.174	378.17	10958	3277
B_2	B	40.97	11.58	0.179	377.26	101907	36173
B_3	B	39.38	9.5	0.145	387.64	57634	18822
B_4	B	38.68	9.96	0.144	373.76	206438	75317
B_1^+	B^+	27.81	9.57	0.081	303.95	3028	857
B_2^+	B^+	34.44	10.98	0.122	322.62	446361	127336
B_3^+	B^+	29.39	10.63	0.093	297.67	737122	245314
B_4^+	B^+	31.53	10.47	0.093	281.74	1163143	339705
B_5^+	B^+	32.87	11.47	0.111	294.42	177679	53930

Table I. List of the 17 studied charcoal samples, detailing its nominal hardness, cross-section, height, mass, estimated density, number of recorded AE hits, and number of waiting times (N) computed at the minimum energy threshold of 0.5 aJ.

The upper panel (a) shows the compressive strain applied by the testing machine, defined as the sample height divided by the original sample height. Panel (b) shows the corresponding evolution of the vertical force as a function of time. Panel (c) shows the energy of the individual hits E_k as vertical lines on a logarithmic scale. Note that the plot can only reflect few of the hits, as many of them overlap. In this particular case the total number of recorded AE hits is 8261, as can be seen in panel (d) that shows the evolution of the cumulative number of hits. Finally in the bottom panel (e) we show the behavior of the rate which, for the purpose of this representation, is estimated as the number of hits in windows of 20 s. Note that the vertical scale is logarithmic and that these estimated rates already span 3 decades.

Shortly after an initial adaptation regime the samples display an elastic regime with a rather monotonous increase in the force. In most cases, already for a compressive strain above 0.95, AE hits occur due to nucleation and growth of microfractures in the sample. The samples then typically enter in a serrated force-deformation curve which reaches a maximum, after which a first big collapse occurs. In some cases the collapse is rather sharp but in others there is a series of several collapses. The compression experiments are finished either when the force decreases below a predefined low value (5 N) or when the compressive strain reaches 0.8.

In order to prepare the catalogues of waiting times, from the hits recorded in each experiment, we consider different energy thresholds, from E_{th} =0.5 aJ to E_{th} =50 aJ. Only hits above threshold are considered in order to evaluate the waiting times. For each experiment, the number of hits with energies above the lowest threshold E_{th} =0.5 aJ is indicated in Tab.I. The combination of 17 experiments and 7 different thresholds renders a total of $n_c = 98$ avalanche catalogues (in some cases the large thresholds render no signals) corresponding to different samples with different hardnesses, which we will systematically fit with a double power-law model. We will denote the sets of waiting times in each catalogue as $\left\{\delta_k^i\right\}$, where the index $i = 1, \cdots, n_c$ indicates the catalogue and the index $k = 1, \cdots, N^i$ indicates the different waiting times in each catalogue.

Although, as explained above, waiting times can theoretically be infinitesimally small, in practice there is an experimental limitation that introduces a minimum cutoff in the observed δ_k values. In order to separate consecutive AE hits, we have required that the voltage from the sensors should remain, at least 200 μs below threshold. This implies that it is impossible to observe waiting times below this value. Moreover, even for waiting times above this value, the fact that hits have a certain duration will introduce a clear undercounting in the statistics, which will be reflected as a decrease of the experimental waiting time histograms for low δ values. Therefore, in order to fit the proposed double power-law model to the experimental data set we should modify the model to include an extra parameter which is the minimum cutoff δ_{min}.

$$g(\delta;\alpha,\beta,\delta_0,\delta_{min}) = \begin{cases} \dfrac{(1-\alpha)(\beta-1)}{\left[(\beta-1)\left(1-\frac{\delta_{min}}{\delta_0}\right)^{1-\alpha}+(1-\alpha)\right]\delta_0}\left(\dfrac{\delta}{\delta_0}\right)^{-\alpha} & \text{if } \delta_{min}<\delta\leq\delta_0 \\ \dfrac{(1-\alpha)(\beta-1)}{\left[(\beta-1)\left(1-\frac{\delta_{min}}{\delta_0}\right)^{1-\alpha}+(1-\alpha)\right]\delta_0}\left(\dfrac{\delta}{\delta_0}\right)^{-\beta} & \text{if } \delta_0<\delta<\infty \end{cases}$$

For the following analysis we have estimated for all the experiments a constant minimum cutoff of $\delta_{min} = 2.5$ ms.

We will fit the double power-law probability density, with three free parameters (α, β, and δ_0) but keeping a constant $\delta_{min} = 2.5$ ms, to each of the n_c sets $\{\delta_k^i\}$, using the Maximum Likelihood (ML) method. This method consists in finding the parameters that maximize the Likelihood function

$$\ln \mathcal{L}_i = \sum_k \ln\left[g(\delta_k^i;\alpha^i,\beta^i,\delta_0^i,\delta_{min}=2.5)\right] \quad (10)$$

The advantage of the ML method is that it is known to be independent of the data representation. Thus the estimated parameters do not depend at all on the details of how the histograms are represented. Furthermore the result does not depend on whether or not a change of variables is performed on the probability density. Thus the parameters α^i, β^i, and δ_0^i fitted to the values $\{\delta_k^i, k=1,\cdots N_i\}$ should be exactly compatible with the parameters γ^i, η^i and r_0^i when the double power-law model (with a maximum cutoff $r_{max} = 1/\delta_{min}$) is fitted to the corresponding values $\{1/\delta_k^i, k = 1\cdots N_i\}$. The maximization procedure is performed by the differential evolution numerical algorithm [27] implemented in the SciPy library for Python. We systematically fit the double power-law to both $\{\delta_k^i\}$ and $\{1/\delta_k^i\}$ and crosscheck the exact correspondence of the exponents up to two decimal digits. If discrepancies are found the numerical maximization is repeated starting from different initial conditions until the agreement is reached.

IV. RESULTS

Fig.3 shows an example of histograms corresponding to sample HB$_3$. On the upper-left panel (a) we show the histograms corresponding to the waiting time distributions calculated with 7 different energy thresholds, as indicated by the legend. On the lower-left panel (c) the corresponding histograms for the rate distributions.

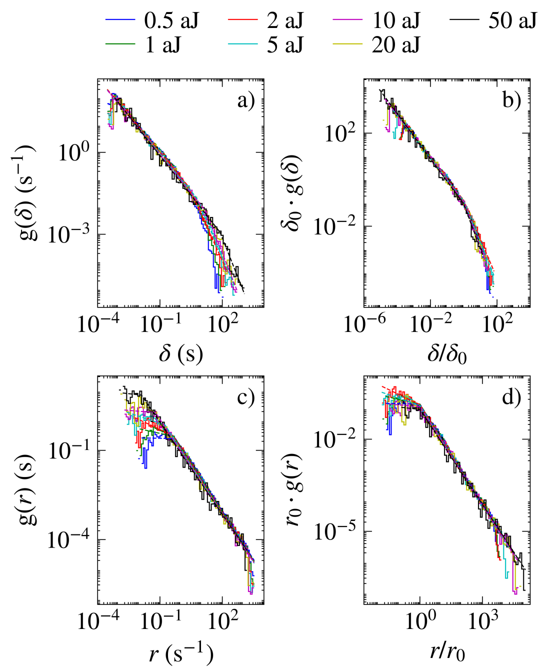

Figure 3. Waiting times and rate distributions corresponding to one sample (HB$_3$). (a) Waiting time histograms for different energy thresholds as indicated by the legend; (b) corresponding scaled waiting times histograms and the corresponding double power-law fits; (c) instantaneous rate histograms; (d) corresponding scaled instantaneous rate histograms and double power-law fits.

At the top of each histogram we show the corresponding ML fitted double power-law models. The values of the fitted δ_0^i and $r_0^i = 1/\delta_0^i$ are used to scale the histograms as shown in the right panels (b) and (d). The corresponding scaled double power-law models are represented with overlapping dashed lines.

As can be seen one obtains slightly different values of the fitted exponents for each histogram. In this particular example we get values $\alpha^i \sim 0.910 - 0.970$, $\beta^i \sim 1.671 - 1.983$, $\gamma^i \sim 0.015 - 0.328$ and $\eta^i \sim 1.030 - 1.091$. Qualitatively similar results are observed for the 17 studied samples.

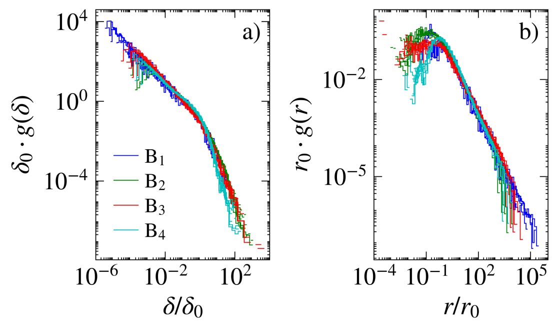

Figure 4. (a) Scaled waiting times histograms corresponding to B samples (B_1, B_2, B_3 i B_4); (b) Corresponding scaled instantaneous rate histograms. The histograms corresponding to the same sample (with different thresholds) are indicated with the same color as indicated in the legend.

A first interesting observation is the fact that, after scaling, histograms overlap rather well thus supporting the USL hypothesis for both $g(\delta)$ and $g(r)$. Note that the scaled distributions for this sample extend for ~ 7 decades. Besides it can be observed that the pure double power-law, with the cusp at the crossover point, reproduces quite well the experimental histograms. Although the differences in the fitted exponents might seem too large, the qualitative comparison with the scaled histograms is good.

The observed fluctuations for the exponent γ^i (of the order of $\sim 100\%$) characterizing the distribution of low rates, are significantly large. This region of rates is the most difficult to study experimentally. Only long enough catalogues with enough mixture of rate activity will allow to observe a good statistical sampling of temporal windows of very low activity.

Fig. 4 illustrates the sample-to-sample variability for the case of four samples obtained from the same original charcoal stick (in this case corresponding to B hardness samples). The samples have very similar heights, crossections and densities as shown in Tab. I.

The histograms corresponding to different energy thresholds of the same sample are represented with the same color to distinguish them from the other samples. As can be seen, after scaling, the sample-to-sample variability (differences between colors) is larger than the variability due to the changes in the energy threshold (observed variations within each color set). Nevertheless, the overall overlap is rather good and qualitatively a pure double power-law model also describes rather well the experimental histograms. This is even true for the large $z = \delta/\delta_0$ region in (a) that shows a power-law decay. Note that the overlap of the scaled histograms spans 10 decades but each color set (each sample) spans fewer decades. This indicates that the different samples, which are, a priori, equivalent, actually have relative waiting times $z = \delta/\delta_0$ which are quite different from sample to sample. This could be due to physical reasons (some samples have different amounts of disorder or are softer than others) or to the fact that for every experiment the coupling of the sensors to the sample might be different. In each experiment the observation window may change.

This is reminiscent of what was found by Corral when studying earthquakes [7]. When waiting time data from different regions of the world were scaled and mixed, the corresponding USL revealed the existence of the second power law decay for large z values.

Fig. 5 shows a summary of all the fitted parameters. The values are represented as a function of the energy threshold and using the same color for the samples with the same hardness. This allows to easily identify if there is any hidden dependence with hardness.

Panel (a) shows the fitted crossover values δ_0^i. As can be seen they are clearly dependent on the energy threshold. The dependence is well described by a power-law behaviour $\delta_0 \sim E^{0.67}$ (as indicated by the dashed straight line in log-log plot). This behaviour is compatible with the existence of a GR exponent $\epsilon = 5/3 \sim 1.67$. The number of events with energy above E_{th} should decrease as $N \sim E_{th}^{-(\epsilon-1)}$. Given the fact that catalogues corresponding to the same sample have the same time duration, it is reasonable to expect that the parameter δ_0 estimating the "mean" waiting time should increase as $\delta_0 \sim E_{th}^{(\epsilon-1)} \simeq E_{th}^{2/3}$.

There might be a certain dependence of δ_0 on the hardness. The softer samples tend to exhibit lower δ_0, but results are not totally conclusive. It could be that given the fact that we are always compressing at a fixed velocity, samples with larger number of signals (in general softer samples) exhibit smaller waiting times. For the other three hardnesses the sample-to-sample variability covers the possible observed dependencies.

Panels (b) and (c) show the behaviour of the exponents α^i and β^i with the threshold E_{th}. As can be seen, although they show a certain dispersion, the values are rather constant.

The values of α^i in Fig. 5(b) range from 0.7 to 1.0 and they might show a certain dependence on hardness. At least for the softer samples they show slightly lower values. With increasing E_{th} there is a tendency for the exponents to increase and a tendency for the overall observed dispersion to reduce. The exponent α describes the small waiting times region. We suggest that these observed small dependencies could have an observational origin related to the minimum time δ_{min}

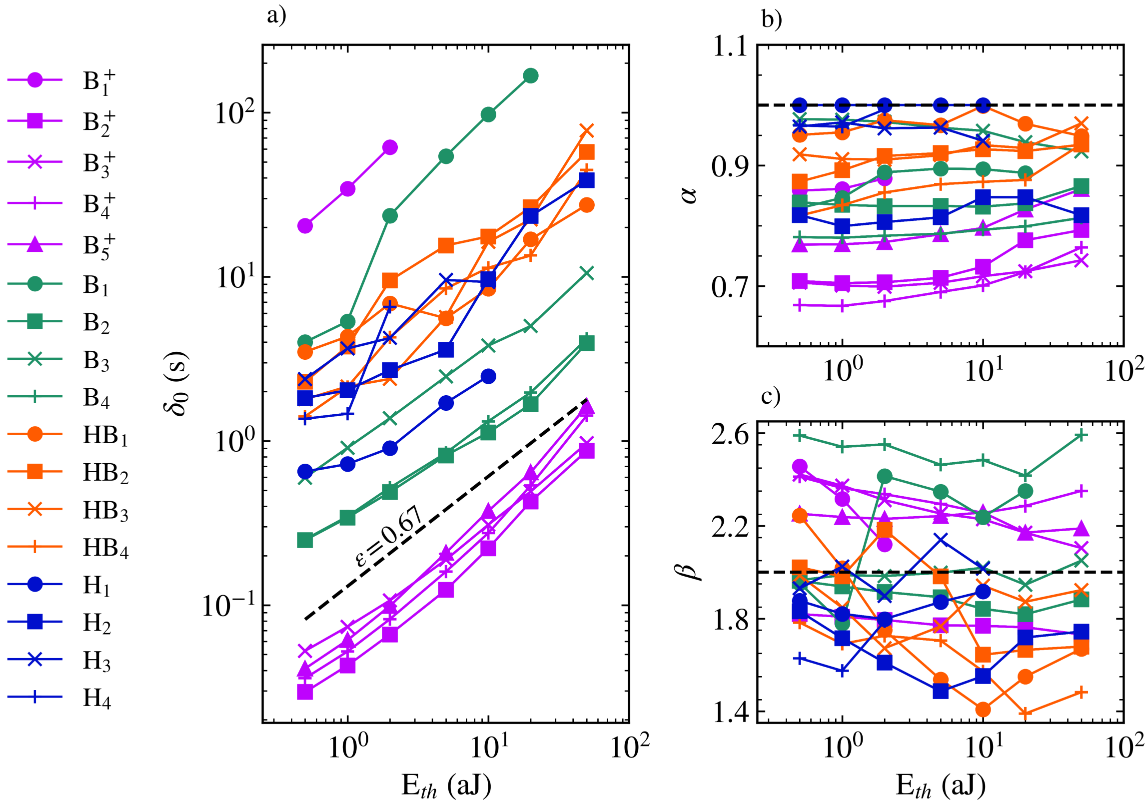

Figure 5. Summary of the fitted parameters as a function of the energy threshold E_{th}: (a) crossover parameter δ_0^i; (b) exponent α^i; (c) exponent β^i. Note that the plots of the exponents in panels (b) and (c) have vertical scales which span 0.5 units and 1.3 units respectively, thus the variability cannot be visually compared.

required to separate events. Such dependence will disappear when E_{th} increases and most of the measured values δ_k^i are much larger than δ_{min}.

Note also that $\alpha = 1$ represents a mathematical limit, above which the double power-law model cannot be normalized. This might explain the tendency of the exponents to concentrate towards $\alpha = 1$ from below but never to overcome it.

The values of β^i in Fig. 5(c) fluctuate between 1.4 and 2.6, with a large sample-to-sample variability and no clear dependence with hardness, nor with E_{th}. This exponent describes the large waiting times distribution. Despite the variability, it is concentrated around $\beta = 2$.

Fig. 6 shows the theoretical regions of the exponent map presented in Fig.1 with the overlapping values of the measured $\alpha^i - \beta^i$ pairs. Despite the large variability, especially for β, the values are concentrated around $\beta = 2$ and $\alpha = 1$.

A similar figure could have been plotted on the $\gamma - \eta$ map, with the exponents concentrated around $\gamma = 0$ and $\eta = 1$.

There is not a straightforward way to combine all the experimental information in order to obtain a common set of exponent values. If we consider the exponents estimated from every cat-

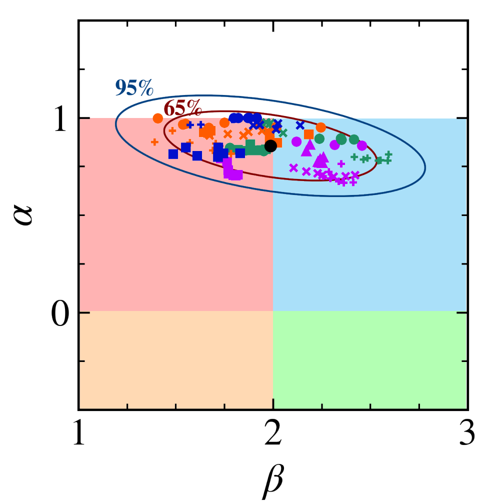

Figure 6. $\alpha - \beta$ exponent diagram with the fitted experimental values. Symbols are indicated in the legend of Fig.5. The coloured regions indicate the regions discussed in Fig.1. The black dot indicates the mean for both exponents, $\bar{\alpha} = 0.86$ and $\bar{\beta} = 2.00$. The ellipses represent the 65% and 95% confidence levels.

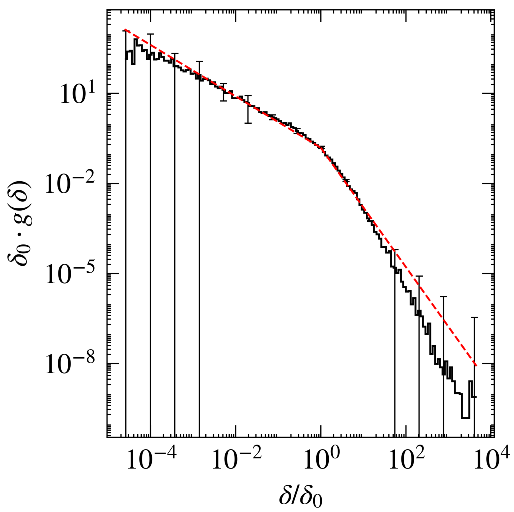

Figure 7. The black line shows the histogram that estimates the distribution of all the scaled waiting times. The red dashed line represents the double power-law model (USL) with exponents $\alpha = 0.86$ and $\beta = 2.00$. Few examples of error bars are shown.

alogue as independent estimations we can evaluate the mean exponents $\bar{\alpha} = 0.86 \pm 0.10$ and $\bar{\beta} = 2.00 \pm 0.29$. These error bars correspond to the standard deviations. Since α and β values show statistical correlation ($\rho = -0.43$) the uncertainties are better described by ellipses in the $\alpha - \beta$ map than by error bars. In Fig. 6 we show the ellipses corresponding to 95% and 65% confidence levels. Note that both ellipses cover the $\alpha = 1$ and $\beta = 2$ point.

In order to compare qualitatively the model with the mean exponents to a "common" histogram, we follow the procedure described in [28]. We first identify different z-segments by ordering the values z^i_{min} in an increasing sequence. On each z-segment, we define logarithmic bins and in order to estimate the probability density we normalize the number of counts on each bin by the number of data recorded in that z-segment and by the bin size.

The common histogram is plotted in Fig.7 together with the model with $\alpha = 0.86$ and $\beta = 2.00$. Some examples of error bars of the histogram are also shown. They have been estimated as the square root of the variance, assuming that the number of counts in each bin follows a binomial distribution. The agreement between the data and the model is quite satisfactory.

V. SUMMARY AND CONCLUSIONS

A double power-law probability density has been proposed to model the distribution of waiting times between avalanches (δ) in a self-organized critical system. The properties of this density have been discussed and compared to the more standard power-law distribution. The double power-law is characterized by two critical exponents α (in the small δ region) and β (in the large δ region) and a crossover parameter δ_0. This distribution shows an interesting symmetry: when exchanging the variables $r = 1/\delta$ one obtains a distribution of instantaneous rates that is also a double power-law with exponents $\gamma = 2-\beta$ for small rate values, $\eta = 2 - \alpha$ for large rate values and $r_0 = \frac{1}{\delta_0}$.

The hypothesis has been tested by studying labquakes in charcoal samples (with different hardnesses) under uniaxial compression. Waiting times catalogues have been obtained considering different energy thresholds.

The results show that the distribution of waiting times are compatible with the double power-law hypothesis with exponents $\alpha \in (0.7, 1.0)$ and $\beta \in (1.4, 2.6)$. The distribution of instantaneous rates can also be described by the corresponding double power-law. The parameter δ_0 depends on the properties of every particular catalogue as well as on details on the observation conditions [14] (e.g., energy threshold or the attenuation of AE). This parameter can be used to scale all the distributions into a unique Universal Scaling Law. We have obtained a best common fit of the exponents $\alpha = 0.86 \pm 0.10$ and $\beta = 2.00 \pm 0.29$. The computed 95% and 65% confidence error ellipses contain the values $\alpha = 1$ and $\beta = 2$ which have been shown to exhibit a particular cancellation of mathematical divergences.

It will be very interesting to investigate whether these conclusions can be extrapolated to avalanches in other self-organized critical systems, especially to earthquakes.

AUTHOR CONTRIBUTION

H.Li did the experimental work including setup and sample preparation, data recording as well as part of the initial analysis. E.Valdés did the major part of the statistical analysis and plots. Conceptualization, design and direction of the experiment was performed by E.Vives who also wrote the first version of manuscript. Data interpretation and the final version of the manuscript was discussed equally by all the authors.

ACKNOWLEDGMENTS

We acknowledge financial support from Spanish Ministry of Science and Innovation

(MCIN/AEI/10.13039/501100011033) and European Union (NextGenerationEU/PRTR) under grants PID2020-113549RB-I00/AEI and TED2021-129952B-C32/AEI and from Generalitat de Catalunya (AGAUR) under grant 2021SGR00328. We acknowledge A. Planes, J.Baró and A.Corral for useful comments.

[1] P.Bak, *How Nature Works: The Science of Self-Organised Criticality* (Copernicus, New York, 1996).
[2] P.Bak, C.Tang, and K.Wiesenfeld, Phys. Rev. Lett. **59**, 381 (1987).
[3] J.P.Sethna, K.A.Dahmen, and C.R.Myers, Nature **410**, 242 (2001).
[4] T.Utsu, Pure and Applied Geophysics **155**, 509 (1999).
[5] T.Utsu, Y.Ogata, and R. Matsu'ura, Journal of Physics of the Earth **43**, 1 (1995).
[6] P.Bak, K.Christensen, L.Danon, and T.Scanlon, Phys. Rev. Lett. **88**, 178501 (2002).
[7] A.Corral, Physica A **340**, 590 (2004).
[8] J.Davidsen and C.Goltz, Geophysical Research Letters **31**, L21612 (2004).
[9] G.Molchan, Pure appl. Geophys. **162**, 1135 (2005).
[10] V.Carbone, L.Sorriso-Valvo, P.Harabaglia, and I.Guerra, EPL **71**, 1036 (2005).
[11] K.Jonsdottir, M.Lindman, R.Roberts, B.Lund, and R.Bodvarsson, Tectonophysics **424**, 195 (2006).
[12] A.Saichev and D.Sornette, Phys. Rev. Lett. **97**, 078501 (2006).
[13] G.Molchan, Pure appl. Geophys. **163**, 1453 (2006).
[14] G.Niccolini, G.Durin, A.Carpinteri, G.Lacidogna, and A.Manuello, J. Stat. Mech. , P010123 (2009).
[15] G.Niccolini, F.Bossia, A.Carpinteri, G.Lacidogna, A.Manuello, and N.Pugno, Phys.Rev.E **80**, 026101 (2009).
[16] S.Abe and N.Suzuki, EPL **97**, 49002 (2012).
[17] A.Celikoglu and U.Tirnakli, Physica A **392**, 4543 (2013).
[18] A.K.Nekrasova and V.G.Kossobokov, Journal of Volcanology and Seismology **14**, 353 (2020).
[19] A.Nekrasova and A.Peresan, Frontiers in Earth Science **8**, 590724 (2021).
[20] J.Baró, Á.Corral, X.Illa, A.Planes, E.K.H.Salje, W. Schranz, D.E.Soto-Parra, and E.Vives, Physical Review Letters **110**, 088702 (2013).
[21] Y.Xu, A.G.Borrego, A.Planes, X.Ding, and E.Vives, Physical Review E **99**, 033001 (2019).
[22] D.Sornette, in *Encyclopedia of Complexity and Systems Science* (Springer, New York, NY, 2007) pp. 7009–7024.
[23] V.Pareto, *Cours d'économie politique* (Laussane: F.Rouge, 1897).
[24] A.A.Toda, Journal of Economic Behavior & Organization **84**, 364 (2012).
[25] A.Corral and A.Gonzalez, Earth and Space Science **6**, 673 (2019).
[26] M.Serra-Peralta, J.Serrà, and A.Corral, Scientific Reports **12**, 2615 (2022).
[27] R.Storm and K.Price, Journal of Global Optimization **11**, 341 (1997).
[28] V.Navas-Portella, I.Serra, A.Corral, and E.Vives, Phys. Rev. E **97**, 022134 (2018).